Co-published by
Institute of Fluid-Flow Machinery
Polish Academy of Sciences
Committee on Thermodynamics and Combustion
Polish Academy of Sciences

http://www.imp.gda.pl/archives-of-thermodynamics/

Multi-optimization of thermodynamic performance of an HT-PEM fuel cell based on MOPSO algorithm

Yuting Wang[a], Zheshu Ma[a*], Yongming Gu[a], Qilin Guo[a]

[a] Nanjing Forestry University, College of Automobile & Traffic Engineering, 210037, China
* Corresponding author email: mazheshu@njfu.edu.cn

Received: 27.03.2024; revised: 09.05.2024; accepted: 12.06.2024

Abstract

In this study, an irreversible thermodynamic model for the high temperature proton exchange membrane fuel cell taking electrochemical and heat losses into account is developed. The power density, exergy destruction index, exergy sustainability index and ecological coefficient of performance is derived. The model was validated against experimental data. The influence of parameters on the irreversible thermodynamic performance of high temperature proton exchange membrane fuel cell are considered. The multi-objective particle swarm optimization algorithm is utilized to optimize the power, ecological coefficient of performance and efficiency. The population distribution of the optimization variables was analyzed using a three-dimensional Pareto frontier analysis, and results show that the maximum power density, maximum efficiency and maximum ecological coefficient of performance being 6340 W/m^2, 64.5% and 1.723 respectively, which are 43.28%, 3.7% and 17.8% higher than the preoptimized high temperature proton exchange membrane fuel cell. Moreover, the nondominated sorting genetic algorithm II and simulated annealing algorithm have been chosen versus multi-objective particle swarm optimization algorithm for making the optimization comparative analysis.

Keywords: HT-PEMFC; Irreversible thermodynamic; Exergy; Parameter optimization; MOPSO algorithm

Vol. 45(2024), No. 3, 197–208; doi: 10.24425/ather.2024.151231

Cite this manuscript as: Wang, Y., Ma, Z., Gu, Y., & Guo Q. (2024). Multi-optimization of thermodynamic performance of an HT-PEM fuel cell based on MOPSO algorithm. *Archives of Thermodynamics*, 45(3), 197–208.

1. Introduction

The high temperature proton exchange membrane fuel cell (HT-PEMFC) is regarded as an alternative device to make up for the shortcomings of PEMFC with the advantages of simpler water and thermal management, faster electrochemical reaction rates and higher utilization of waste heat [1]. However, it is accompanied by significant irreversible thermal losses which lead to limit the broader application of HT-PEMFC [2–4].

Irreversible thermodynamic loss refers to the energy loss that occurs in the process of energy conversion or transfer that is not completely recoverable [5]. In thermodynamic systems, irreversible processes lead to an increase in the entropy of the system, which results in thermodynamically irreversible losses. Regarding fuel cells, irreversible thermodynamic losses are inevitably caused by heat transfer and chemical reactions in the system, such as polarization losses caused by the electrochemical reaction process of the fuel cell, heat losses that cannot be converted into electrical energy during the working process, and resistance losses caused by the current passing through the resistive elements in the cell. These irreversible thermodynamic losses have a significant impact on the performance and efficiency of fuel cells, which can be minimized by optimizing the

Nomenclature

A – activation area, cm^2
C_p – constant specific heat of the gas, J/(kg K)
DL – phosphate doping level
E – potential, V
Ex – exergy, W/m^2
e_n^{ch} – chemical exergy, J/mol
F – Faraday's constant, C/mol
f_{exd}^{fc} – exergy dissipation rate
ΔG – Gibbs free energy change, J/mol
$\Delta \dot{H}$ – enthalpy transition, W/m^2
j – current density, A/m^2
K – specific heat rate, J/(kg K)
n – number of electrons transferred
P – power density, W/m^2
p – pressure, atm
R – gas constant, J/(mol K)
RH – relative humidity, %
r – waste exergy ratio
ΔS – variation of standard molar entropy, J/mol
T – operating temperature, K
T_0 – ambient temperature, K
t – thickness, cm
U – voltage, V
x_n – mole fraction

Greek symbols

α – transfer coefficient
$\dot{\delta}$ – entropy production
η_{ex}^{fc} – exergy efficiency
σ – proton conductivity, S/m

Subscripts and superscripts

act – activation
ch – chemical
con – concentration
d – dissipation
fc – fuel cell
mem – membrane
ohm – ohmic
ph – physical
rev – reversible
rw – recyclable exergy waste
uw – unrecyclable exergy waste
w – waste exergy

Abbreviations and Acronyms

HT-PEMFC– high temperature proton exchange membrane fuel cell
ECOP – ecological coefficient of performance
EDI – exergy destruction index
ESI – exergy sustainability index
MOPSO– multi-objective particle swarm optimization
NSGA – nondominated sorting genetic algorithm
ORC – organic Rankine cycle
PBI – polybenzimidazole
SA – simulated annealing

design and improving the materials to achieve higher efficiency and performance of fuel cells [6]. A large number of researchers have made efforts to find more efficient materials and design methods in order to minimize these losses and improve the sustainability of fuel cells [7–9].

Numerous studies have been conducted to analyze and optimize the irreversible performance of fuel cells according to the first and second laws of thermodynamics. Atak et al. [10] investigated the thermodynamic performance of PEMFC using energy analysis and exergy analysis under a certain range of temperature and pressure, and the results showed that increasing the temperature improves the power density and exergy efficiency, and increasing the current density leads to an improvement in the entropy production, however, the effect of the pressure change on the irreversibility of PEMFC is not as visible as that of the temperature. Chen et al. [11] established a degradation model for predicting the lifetime of PEMFC and analyzed the thermodynamic performance during the whole lifetime based on the model, as well as discussing the influence of various currents on power, degradation rate and thermal efficiency. Lu et al. [12] proposed a PEMFC and organic Rankine cycle (ORC) cogeneration system to generate electricity by recovering the waste heat from the fuel cell stack through the ORC subsystem, and analyzed the thermodynamic performance under steady state and dynamic conditions based on this system. The results show that the exergy efficiency of this PEMFC system can reach 51% and the energy efficiency can reach 75%, and the rate of electric efficiency decrease with increasing current is reduced. Tayfun Özgür end Yakaryilmaz [13] investigated the energy and exergy performance of a PEMFC with output power of 1 kW, and the experimental results showed that the energy efficiency of the PEMFC was 45.58%, and that increasing the temperature and pressure allowed an increase in the physical exergy of all the reactants and products.

The performance can be significantly improved by numerically analyzing and optimizing the operating and design parameters of the PEMFC, which is a well-designed approach to save experimental expenses and time, and is more conducive to overall energy efficiency than time-consuming and laborious experimental studies. A large number of researchers have studied fuel cells using advanced optimization algorithms and parametric analysis methods [14,15]. Chen et al. [16] analyzed the electrochemical and thermodynamic properties of PEMFC using parametric studies, and achieved efficiency and power improvement by optimizing the operating parameters of PEMFC using a novel evolutionary algorithm, and the final optimization results showed that the energy efficiency of PEMFC could reach 79% and the power could reach 8.04 kW. Xu et al. [17] investigated the effects of operating parameters on the irreversibility and exergy performance of HT-PEMFC under different operating conditions and optimized the performance of HT-PEMFC using Manta Ray Foraging Optimization Algorithm. Lin et al. [18] analyzed the exergy efficiency of HT-PEMFC using the meta-heuristics method as well as evaluated and optimized the thermodynamic irreversibility of HT-PEMFC using an improved collective animal behavior algorithm. The results show that the algorithm has stronger convergence speed and optimization efficiency compared to the genetic algorithm. It is evident from pre-

vious studies that optimization of parameters to match the best operating conditions of the HT-PEMFC can reduce irreversible losses and improve efficiency.

The multi-objective particle swarm optimization (MOPSO) is to use the external population archive to store all the current non-dominated solutions, and regard the individuals in the external archive as the elite individuals, control the direction of population evolution through the elite individuals, and guide the population to approximate the real Pareto frontier, and take the particles in the external archive as the obtained approximation of the Pareto optimal solution at the end of the algorithm operation. The MOPSO algorithm has been widely used in the energy field to solve multi-objective optimization problems. Ehyaei et al. [19] used MOPSO algorithm to optimize the thermodynamic performance of parabolic through collector based on energy, exergy and economic analysis, and the optimal results were calculated with maximum exergy efficiency and minimum heat generation. Yuan et al. [20] designed an optimization algorithm based on the MOPSO algorithm and grey correlation analysis, as well as employed this algorithm to optimize a multi-objective energy scheduling problem for a hybrid solid oxide fuel cell and solar hybrid cogeneration system.

Few literatures about ecological performance analysis in HT-PEMFC have been published by far and even fewer papers focus on the ecological coefficient of performance (ECOP) as an optimization function for the thermodynamic performance of HT-PEMFC. The ECOP is an important evaluation index for irreversible thermodynamic and ecological performance, and optimizing ECOP can reduce power loss to benefit the environment. Therefore, in this paper, the ECOP, P and efficiency as the multi-objective optimization function for analyzing and optimizing the thermodynamic performance while maintaining the power of HT-PEMFC is still required. The population distribution of the optimization variables was analyzed using a 3D Pareto frontier analysis, and the popular nondominated sorting genetic algorithm II (NSGA-II) and simulated annealing algorithm (SA) have been chosen versus MOPSO algorithm for making the optimization comparative analysis.

2. Model development

The principles of redox reactions can be simplified and stated as follows [16]:

$$\mathrm{H_2} \rightarrow 2\mathrm{H^+} + 2e^-, \tag{1}$$

$$2\mathrm{H^+} + \frac{1}{2}\mathrm{O_2} + 2e^- \rightarrow \mathrm{H_2O} + \text{heat}, \tag{2}$$

$$\mathrm{H_2} + \frac{1}{2}\mathrm{O_2} \rightarrow \mathrm{H_2O} + \text{heat} + \text{electricity}. \tag{3}$$

In addition, some assumptions about modeling are provided below:

- The HT-PEMFC is operated in steady state [4].
- The fuel is a mixture of hydrogen and water [21].
- The movement of reactants exhibits laminar flow [10].
- The consideration of kinetic and potential energy of hydrogen is omitted [16].
- The corrosion reactions at the electrodes are neglected [22].

The values of basic designing and operating parameters used in this paper are obtained from Ref. [22], which can be shown in Table 1.

Table 1. Operating and design parameters [22].

Parameter	Value	Unit	Parameter	Value	Unit
T	413~473	K	R	8.314	J/(mol·K)
p	1~3	atm	j	0~20000	A/m²
RH	0~7.6	%	T_0	298.15	K
DL	2~10	-	α	0.25	-
t_{mem}	0.005	cm	n	2	-
F	96485	C/mol	A_{mem}	600	cm²

2.1. Electrochemical description

The reversible voltage E_{rev} can be calculated by [1]:

$$E_{rev} = E_r^0 + \frac{\Delta S}{nF}(T - 298.15) + \frac{RT}{n_e F}\ln\left(\frac{p_{\mathrm{H_2}} p_{\mathrm{O_2}}^{0.5}}{p_{\mathrm{H_2O}}}\right), \tag{4}$$

where E_r^0 is the ideal standard potential, R is the gas constant, ΔS is the variation of standard molar entropy, T is the temperature. The correlation between ΔS and T reads:

$$\frac{\Delta S}{n_e} = -18.449 - 0.01283T. \tag{5}$$

(1) Activation overpotential

The E_{act} taking the effect of leakage current into account can be calculated by:

$$E_{act} = \frac{RT}{\alpha nF}\ln\left(\frac{j + j_{leak}}{j_0}\right), \tag{6}$$

where α is the transfer coefficient, j is the current density, j_{leak} is the leakage current density, j_0 is the exchange current density. The correlation between j_{leak} and T is calculated by [2]:

$$\ln j_{leak} = -2342.9\left(\frac{1}{T}\right) + 9.0877. \tag{7}$$

(2) Ohmic overpotential

The E_{ohm} is given by:

$$E_{ohm} = j(R_{ion} + R_{ele}) = jR_{ion} = j\frac{t_{mem}}{\sigma_{mem}}, \tag{8}$$

where t_{mem} is the thickness of the membrane, σ_{mem} is the proton conductivity.

(3) Concentration overpotential

The E_{con} is expressed as [3]:

$$E_{con} = \left(1 + \frac{1}{\alpha}\right)\frac{RT}{nF}\ln\left(\frac{j_L}{j_L - j}\right), \tag{9}$$

where j_L is the limiting current density.

The total internal resistance due to these three overpotentials can be calculated by:

$$R_{int} = \frac{E_{act} + E_{ohm} + E_{con}}{A_{mem} j}, \tag{10}$$

where A_{mem} is the activated area.

Combining Eqs. (6)–(10), the voltage U can be calculated as:

$$U = E_{rev} - \left(1 + \frac{1}{\alpha}\right)\frac{RT}{nF}\ln\left(\frac{j_L}{j_L - j}\right) - \frac{RT}{\alpha nF}\ln\left(\frac{j + j_{leak}}{j_0}\right) - j\frac{t_{mem}}{\sigma_{mem}}. \quad (11)$$

The power density can be calculated as:

$$P = jU = j(E_{rev} - E_{con} - E_{act} - E_{ohm}). \quad (12)$$

2.2. Thermodynamic description

When fuel cell operates, oxygen and hydrogen interact in a redox reaction [11], and the total energy released by the electrochemical reaction is equivalent to enthalpy variation, i.e. $-\Delta\dot{H}$, which can be calculated by:

$$-\Delta\dot{H} = -\frac{jA\Delta h}{nF}. \quad (13)$$

The $-\Delta\dot{H}$ can be described by:

$$-\Delta\dot{H} = -\Delta G - T\Delta S. \quad (14)$$

Total energy can be categorized into electrical energy and thermal energy, which is due to the enthalpy variation being lower than the Gibbs free energy, and a portion that cannot be converted to electricity is released to thermal energy [4]. This fraction is denoted by $-\Delta G + \Delta\dot{H}$, which is equal to $T\Delta S$, and ΔS is called the entropy [2].

Based on the laws of thermodynamics, thermal efficiency can be calculated by [2]:

$$\eta = \frac{P}{-\Delta\dot{H}}. \quad (15)$$

Based on the representation of *ECOP* in Ref. [5], it can be calculated by:

$$ECOP = \frac{PT}{T_0(-\Delta\dot{H} - P)}. \quad (16)$$

ECOP is a crucial irreversible thermodynamic indicator due to the advantage of compromising the weights of power and efficiency.

Moreover, the exergy analysis of irreversible thermodynamics is used to study and optimize the recoverable energy and unrecoverable losses during fuel cell operation [6]. The exergy balance can be represented as:

$$Ex_{in}^{fc} = P + Ex_{w,out}^{fc} + Ex_d^{fc}, \quad (17)$$

where Ex_{in}^{fc} is the total input exergy, $Ex_{w,out}^{fc}$ is the waste exergy, and Ex_d^{fc} is the exergy dissipation.

Therefore, the exergy dissipation can be obtained as:

$$Ex_d^{fc} = Ex_{in}^{fc} - P - Ex_{w,out}^{fc}. \quad (18)$$

Recoverable exergy wastes are losses that can be recycled, e.g. remaining hydrogen can be recycled and used to generate energy [6], the unrecoverable exergy waste is a loss that cannot be reused, such as waste heat:

$$Ex_{w,out}^{fc} = Ex_{rw}^{fc} + Ex_{uw}^{fc}, \quad (19)$$

where Ex_{rw}^{fc} is the recoverable exergy, and Ex_{uw}^{fc} is the unrecoverable exergy.

The recoverable exergy is mainly the chemical exergy of the remaining hydrogen and oxygen and can be expressed as:

$$Ex_{rw}^{fc} = n_{\mathrm{H}_2,out} \cdot ex_{\mathrm{H}_2,out}^{ch} + n_{\mathrm{O}_2,out} \cdot ex_{\mathrm{O}_2,out}^{ch}, \quad (20)$$

where $n_{\mathrm{H}_2,out}$ is the mole fraction of hydrogen, $ex_{\mathrm{H}_2,out}^{ch}$ is the standard chemical exergy of hydrogen, $n_{\mathrm{O}_2,out}$ is the mole fraction of oxygen, and $ex_{\mathrm{O}_2,out}^{ch}$ is the standard chemical exergy of oxygen.

The unrecoverable exergy is mainly the physical exergy of the discharged hydrogen, oxygen and water as well as the waste heat, and can be expressed as [1]:

$$Ex_{uw}^{fc} = (n_{\mathrm{H}_2,out} \cdot ex_{\mathrm{H}_2,out}^{ph} + n_{\mathrm{O}_2,out} \cdot ex_{\mathrm{O}_2,out}^{ph} + \\ + n_{\mathrm{H_2O},out} \cdot ex_{\mathrm{H_2O},out}^{ph}) + Q_{w,out}^{fc}\left(1 - \frac{T_0}{T}\right), \quad (21)$$

where $n_{\mathrm{H_2O},out}$ is the mole fraction of water, $ex_{\mathrm{H_2O},out}^{ph}$ is the standard chemical exergy of water, and $Q_{w,out}^{fc}$ is the waste heat of the fuel cell.

The exergy destruction index *EDI* is used to numerically describe the environmental impact of unrecoverable exergy losses in this paper, and larger values of *EDI* indicating that the irreversible thermodynamic process is more damaging to environment; it can be calculated by [7]:

$$EDI = \frac{Ex_{uw}^{fc} + Ex_d^{fc}}{P}. \quad (22)$$

The exergy sustainability index *ESI* can be calculated by [2]:

$$ESI = \frac{P}{EDI \cdot (P + Ex_{w,out}^{H_2} + Ex_{w,out}^{O_2} + Ex_d^{fc})}. \quad (23)$$

2.3. MOPSO optimization

2.3.1. Description of MOPSO algorithm

The MOPSO is a bionic algorithm derived from imitating the hunting behaviour of birds, which is based on the principle of randomly distributing a certain number of particles in the feasible domain, and each particle flies at a certain speed and direction and adjusts the direction and speed of the next moment by combining with its own current optimal position and the optimal position of the group, and ultimately achieves the purpose of searching for the optimal solution domain [8].

Suppose the search space is D dimensional and the entire particle population is N_S, the velocity and position of the particle i at the t iteration are $v_i^t = (v_{i,1}^t, v_{i,2}^t, \ldots, v_{i,D}^t)$, and $x_i^t = (x_{i,1}^t, x_{i,2}^t, \ldots, x_{i,D}^t)$, respectively; the optimal position searched so far by the particle i at the t iteration is $p_i^t = (p_{i,1}^t, p_{i,2}^t, \ldots, p_{i,D}^t)$, i.e. the personal best position; the optimal position searched so far by the population at the t iteration is $g^t = g_1^t, g_2^t, \ldots, g_D^t, ,$ i.e. the global best position. At the $t+1$ iteration, the particles adjust their forthcoming velocity and location in the search space, incorporating insights gained from their personal history as well as the sharing experiences of the

entire population [8,9]. The velocity and position updates of the particle swarm optimization algorithm with inertia weights can be represented by Eq. (24) and (25), respectively:

$$v_{i,j}^{t+1} = \omega^* v_{i,j}^t + c_1 r_1 (p_{i,j}^t - x_{i,j}^t) + c_2 r_2 (g_j^t - x_{i,j}^t), \quad (24)$$

$$x_{i,j}^{t+1} = x_{i,j}^t + v_{i,j}^{t+1}, \quad (25)$$

where t is the number of iterations, c_1, c_2 are constants, r_1, r_2 are random numbers, ω^* is the inertia weight, $p_{i,j}^t$ is the individual position, g_j^t is the global optimum position, and $j = 1,2,\ldots,D$ is the dimension.

The position of the particle is updated schematically as shown in Fig. 1.

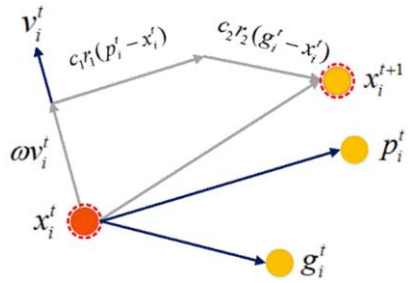

Fig. 1. Schematic diagram for updating the position of a particle.

2.3.2. Determination of optimization variables and objective function

Considering that the thermodynamic performance of HT-PEMFC is affected by multiple parameters and there are various indexes to evaluate the irreversible loss in the working process from different perspectives, and that each performance evaluation index has its advantages and imperfections. Based on the established model and previous studies, it is seen that the operating and design parameters such as the temperature T, pressure p, relative humidity RH, and phosphate doping level DL have a large impact on the performance of the HT-PEMFC, and different configurations of the operating parameters determine the output performance of the HT-PEMFC. Therefore, in this paper, not only the effects of the above parameters on the thermodynamic performance of HT-PEMFC are analyzed, but also these parameters are used as optimization variables to improve the thermodynamic performance of HT-PEMFC. Moreover, the power P and efficiency η are the most widely used basic metrics for evaluating fuel cells, while $ECOP$ is an important indicator in thermodynamics to quantify the irreversible thermodynamic loss of fuel cells; therefore, the P, efficiency η, and $ECOP$ are selected as the objective functions in order to improve the output performance of the HT-PEMFC in a more comprehensive way and to reduce the irreversible thermodynamic loss in this paper. The range of the determined optimization variables and the objective function are shown in Table 2.

Table 2. The optimization variables and the objective function.

Optimization variables and ranges		Objective function
T	413~473 K	P
p	1~3 atm	η
RH	0~7.6 %	$ECOP$
DL	2~10	-
j	0~20000 A/m^2	-

The flowchart of the MOPSO algorithm is shown in Fig. 2. The optimization procedure is as follows:

1) Initialize the random parameters, and create the external archive.
2) Calculate the objective function of the particle swarm. Evaluate the particles and conduct Pareto sorting.

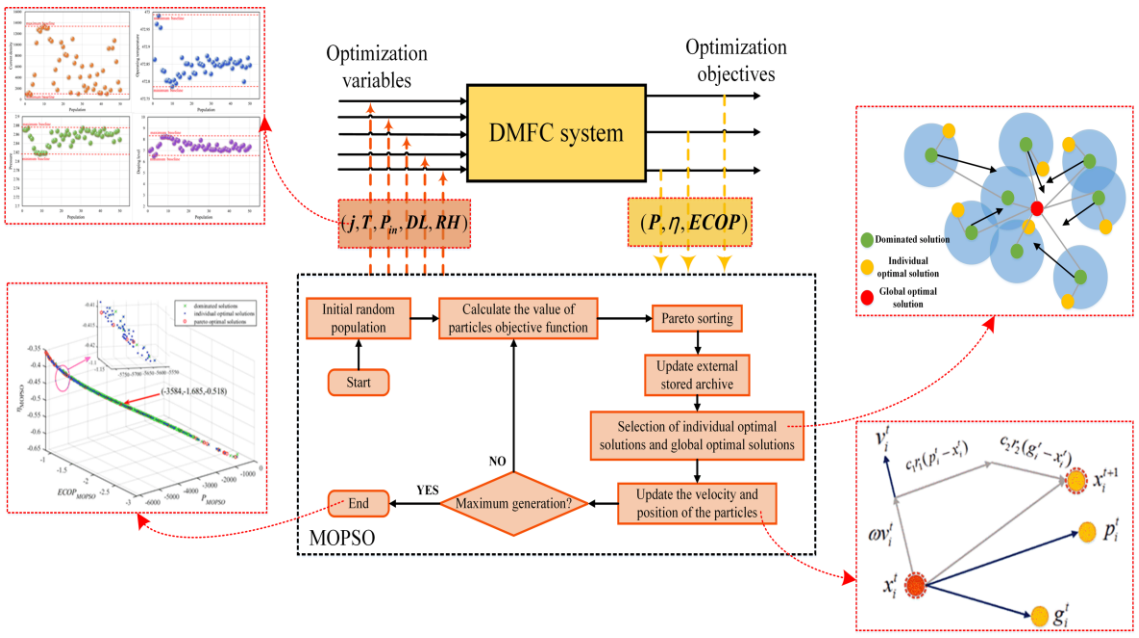

Fig. 2. The flowchart of the MOPSO algorithm.

3) Store the non-dominated solutions into the external archive and update it.
4) Select the individual optimal solution and the global optimal solution.
5) Update the velocity and position of the particles.
6) Return to 2) if the maximum iteration is not reached, and exit the loop if the maximum iteration is reached.

3. Results and discussion

3.1. Validation of the HT-PEMFC model

The output voltage of HT-PEMFC versus j found based on the above equations for the E_{rev}, E_{con}, E_{ohm}, E_{act} is illustrated in Fig. 3a To verify the *U-I* curve, Fig. 3b shows the comparison between model predictions and experimental data of Scott et al. [10]. It can be seen that the theoretical predictions are basically consistent with the experimental data.

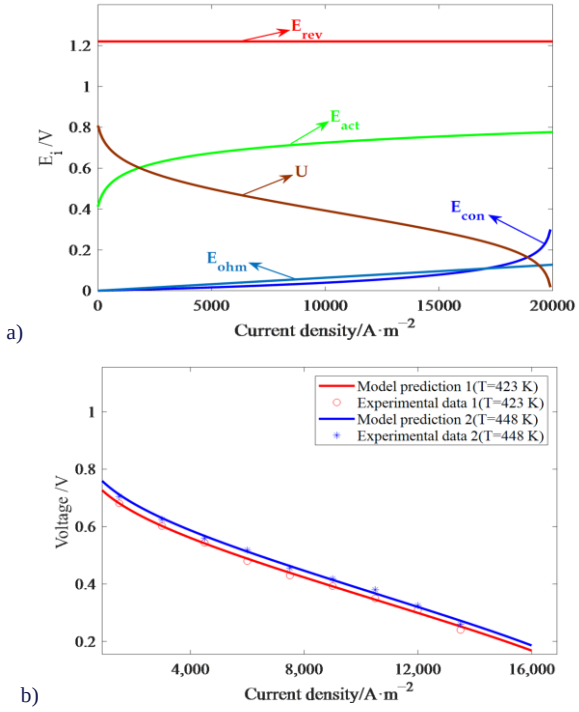

Fig. 3. The model validation: a) curves of potential, activation overpotential, concentration overpotential, ohmic overpotential and voltage versus current density, b) comparison of curves between model results and experimental data.

3.2. Effect of operating and design parameters

It can be seen from Fig. 4a and Fig. 4b that increasing the temperature of HT-PEMFC has an obvious effect on *P*, *ECOP* and *EDI*, mainly due to the fact that the increase in temperature enhances the catalytic activity of the electrodes, which accelerates the redox reaction rate of hydroxide. The maximum power density can reach 5300 W/m^2 when the temperature is 473 K, which is an increase of 58.3% compared to when the temperature is 413 K. As the electrochemical reaction proceeds, *P*, *ESI* and *ECOP* are significantly enhanced by increasing temperature, but *EDI* is decreased, this is due to the fact that the elevation of *T* greatly enhances the electrochemical reaction rate, which reduces the fuel emissions and facilitates the reduction of the loss of exergy and the impact on the environment.

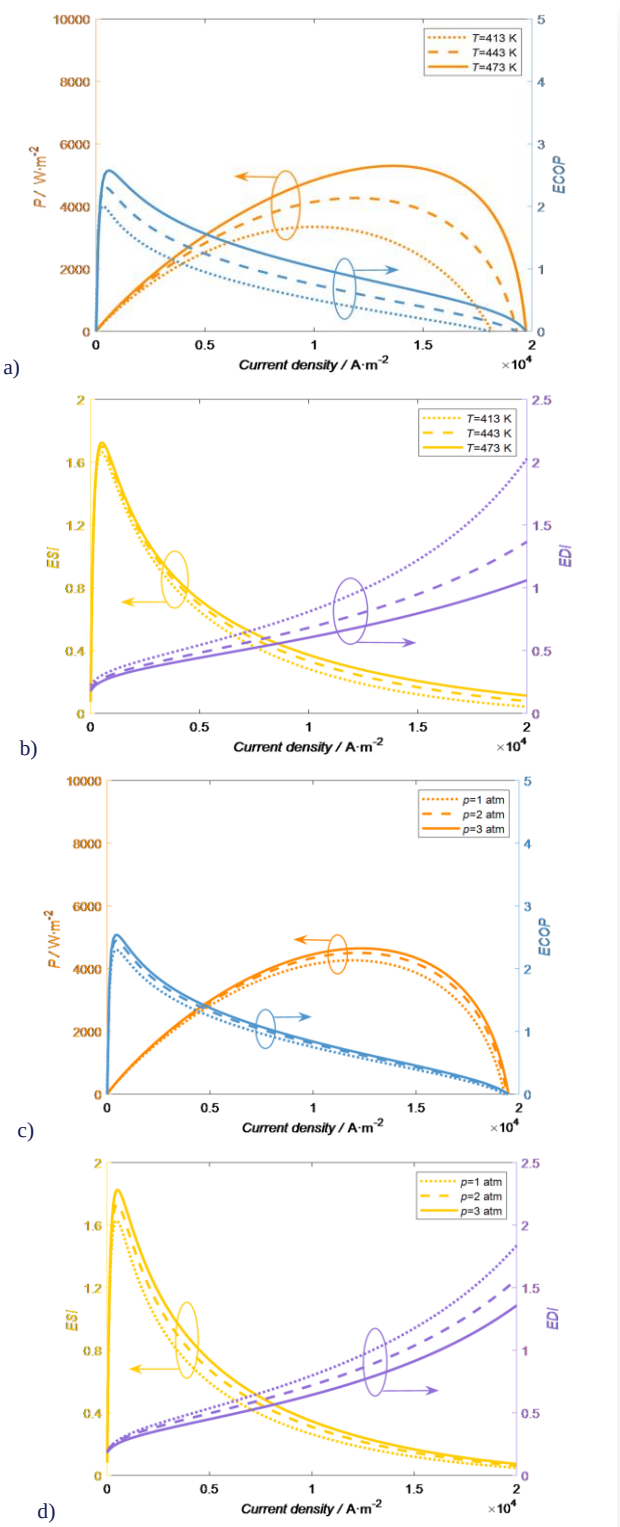

Fig. 4. Curves of *P* and *ECOP* versus current density under: a) different operating temperature, c) different operating pressure. Curves of *ESI* and *EDI* versus current density under: b) different temperature, d) different pressure.

From Figs. 4c and 4d, the maximum power density can reach 4648 W/m^2 when the pressure is 3 atm, which is an increase of 8.9% compared to when the operating pressure is 1 atm. It is

clear that *P*, *ECOP*, *ESI* and *EDI* are less affected by pressure in the range of low current densities, which is due to the low rate of electrochemical reaction. The rate of electrochemical reaction is rising very quickly in the range of high current densities, the irreversible losses are reduced by increasing pressure.

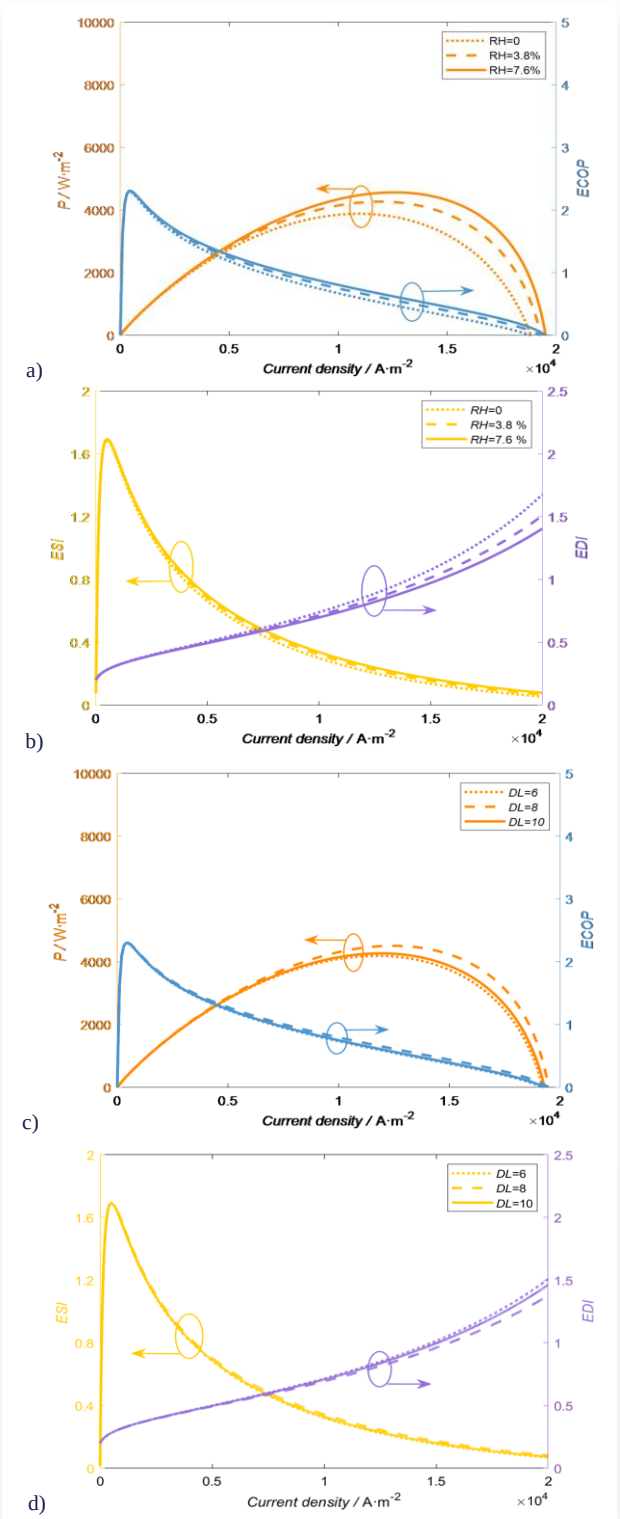

Fig. 5. Curves of *P* and *ECOP* versus current density under: a) different relative humidity, c) different *DL*. Curves of *ESI* and *EDI* versus current density under: b) different relative humidity, d) different *DL*.

The proton conductivity is increased by improving relative humidity, as shown in Fig. 5a and Fig. 5b, where *P* and *ECOP* are enhanced by increasing relative humidity.

When the relative humidity is 7.6%, the maximum power density of HT-PEMFC can reach 4565 W/m^2, which is an increase of 17.7% compared to when the relative humidity is zero. As illustrated in Fig. 5c and Fig. 5d, *P*, *ECOP* and *ESI* first grow and then fall with the rise of *DL*, reaching a maximum at *DL* of 8. A proper increase in *DL* can help to improve proton conductivity while reducing irreversible losses. However, excessive *DL* can damage the structure of PBI, such as affecting the attachment rate of phosphoric acid on the catalytic layer, and resulting in a decrease in proton conductivity [7].

3.3. Optimization results

The optimized Pareto frontier curve of the MOPSO algorithm is shown in Fig. 6. The green fork represents the dominated solutions of the MOPSO algorithm, the blue dots are the individual optimal solutions, and the red hexagrams are the non-dominated group optimal solutions, i.e. the Pareto frontier. Because the MOPSO algorithm procedure used in this paper is a minimum value seeking method, the function set in this procedure is the opposite of the objective function, i.e. $P_{MOPSO}(x_k) = -P(x_k)$, $ECOP_{MOPSO}(x_k) = -ECOP(x_k)$, $\eta_{MOPSO}(x_k) = -\eta(x_k)$, thus seeking the maximum value of the original function, therefore the axis in Fig. 6 is minus. Since the three optimization objective functions of *P*, efficiency and *ECOP* are taken into account, the final optimization result should not only be picked in the Pareto frontier, but also satisfy that each objective function should not be worse. Therefore, after carrying out several optimizations, we chose the Pareto point with the coordinates of –3584, 1.685, −0.518, and its corresponding values of the optimal parameter variables are shown in Table 3.

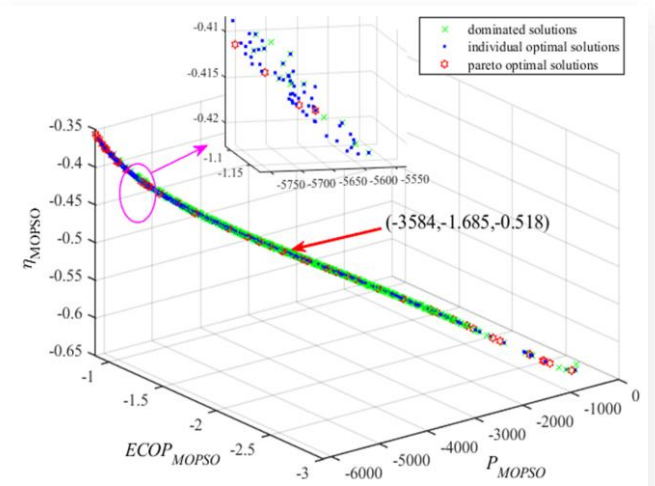

Fig. 6. The optimized Pareto frontier curve of the MOPSO algorithm.

The population distribution of the optimization variables corresponding to the Pareto optimal solutions is shown in Fig. 7. The distribution of current densities is shown in Fig. 7a, and it can be seen that the current densities corresponding to the optimal solutions obtained from the MOPSO optimization are uniformly distributed between 0 and 14000 A/m^2, which is due to

the optimal solutions of the multi-objective optimization selecting different values of weights for each objective. The distribution of operating temperatures is shown in Fig. 7b, and it can be seen that most of the temperatures corresponding to the optimal solutions are between 472.8 K and 472.9 K, which indicates that higher temperatures are useful for the power, efficiency and *ECOP*. The distribution of pressures is shown in Fig. 7c, and it can be seen that most of the pressures corresponding to the optimal solutions are in the range of 2.82 atm to 2.88 atm, which indicates that higher pressures are beneficial for improving performance. The distribution of *DL* is shown in Fig. 7d, and most of the pressures corresponding to the optimal solutions are between 7 and 8, which shows that the *DL* should not be either excessive or insufficiently low for improving irreversible thermodynamic performance.

Table 3. Optimal parameter selection for HT-PEMFC.

	Preoptimized	MOPSO	NSGA-II	SA1	SA2	SA3
Objectives	-	*P, ECOP, η*	*P, ECOP, η*	*P*	*ECOP*	*η*
***j* (A/m²)**	0~20000	7825	6629	13974	5994	6069
***T* (K)**	443	472.88	471.98	469.08	462.00	464.20
***p* (atm)**	2	2.98	2.92	3.00	2.66	3.00
***RH* (%)**	3.8	7.15	7.20	7.48	7.52	7.11
DL	6	8.23	7.90	8.37	9.00	7.60

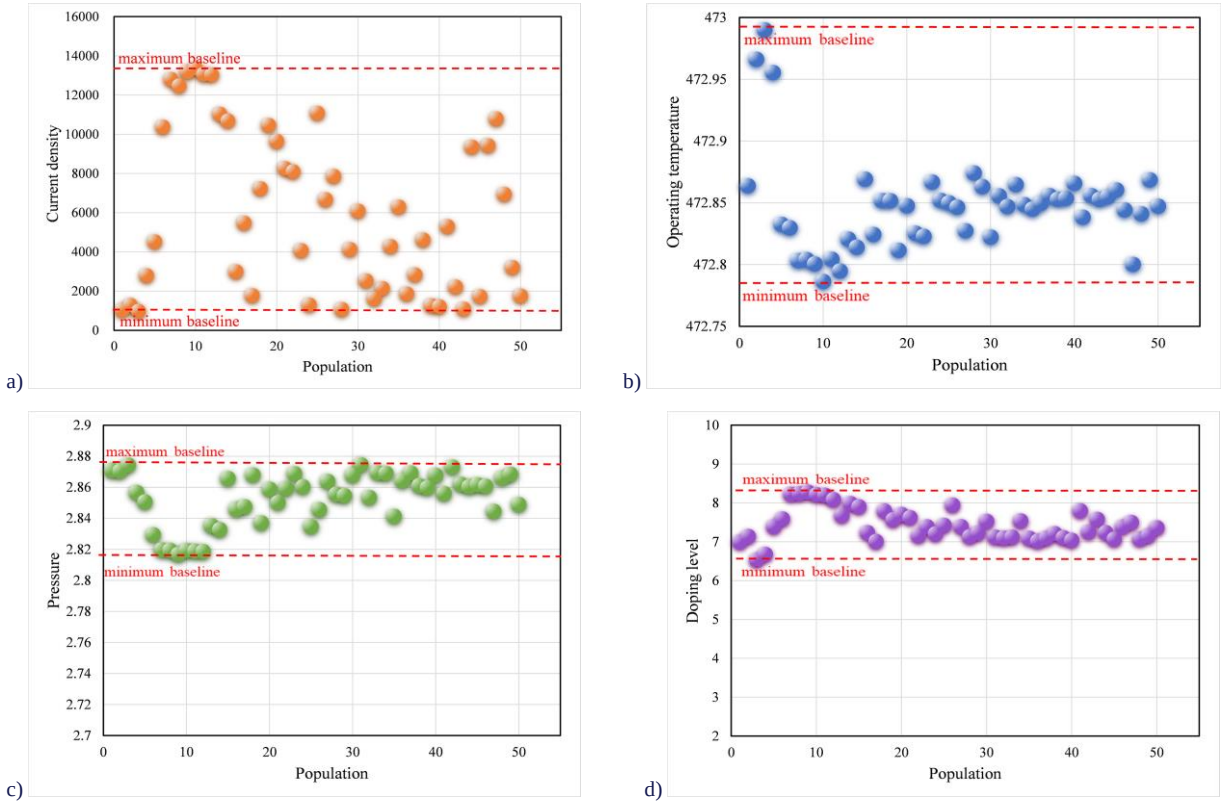

Fig. 7. Population distributions of current density (a), operating temperature (b), pressure (c) and doping level (d).

The optimized Pareto frontier curve of NSGA-II algorithm is shown in Fig. 8a, the red pentagrams are the Pareto frontier of multi-objective optimization, after performing several optimizations, we chose the Pareto point with the coordinates 3088, 1.87, 0.5413, and the values of the optimal parameter variables corresponding to it are shown in Table 3.

The optimization results of the SA algorithm are shown in Figs. 8b, 8c and 8d. In this study, the SA algorithm is a single objective optimization algorithm. Therefore, the optimization objective functions are power density, *ECOP* and efficiency, and the optimized solutions tend to be stable after several optimizations. The three optimal solutions with power density, *ECOP* and efficiency as the optimization objective functions are 6281.67 W/m^2, 1.617 and 51.1%, respectively, and the corresponding values of the optimal parameter variables are shown in Table 3.

In order to compare the convergence speed and optimization accuracy of two multi-objective algorithms more precisely, the Ackley test function is introduced in this paper for comparative analysis, which can detect the global convergence speed of an algorithm. The directional gradients of the Ackley function are various when the dimension increases. As shown in Fig. 9 for

the graph of Ackley, it can be seen that its minimal value is 0. The optimization algorithm can easily fall into the trap of local minimal value. In order to fairly evaluate the advantages and disadvantages of the algorithms, the number of iterations set are all 500, and the population size are all 100. In the NSGA-II algorithm involving crossover probability and mutation probability, are set to 0.7 and 0.01, respectively. whereas in the MOPSO algorithm involving the initial inertia factor weights are set to 0.9, and the inertia factor at the time of iterating to the maximum number of evolutionary generations is 0.4.

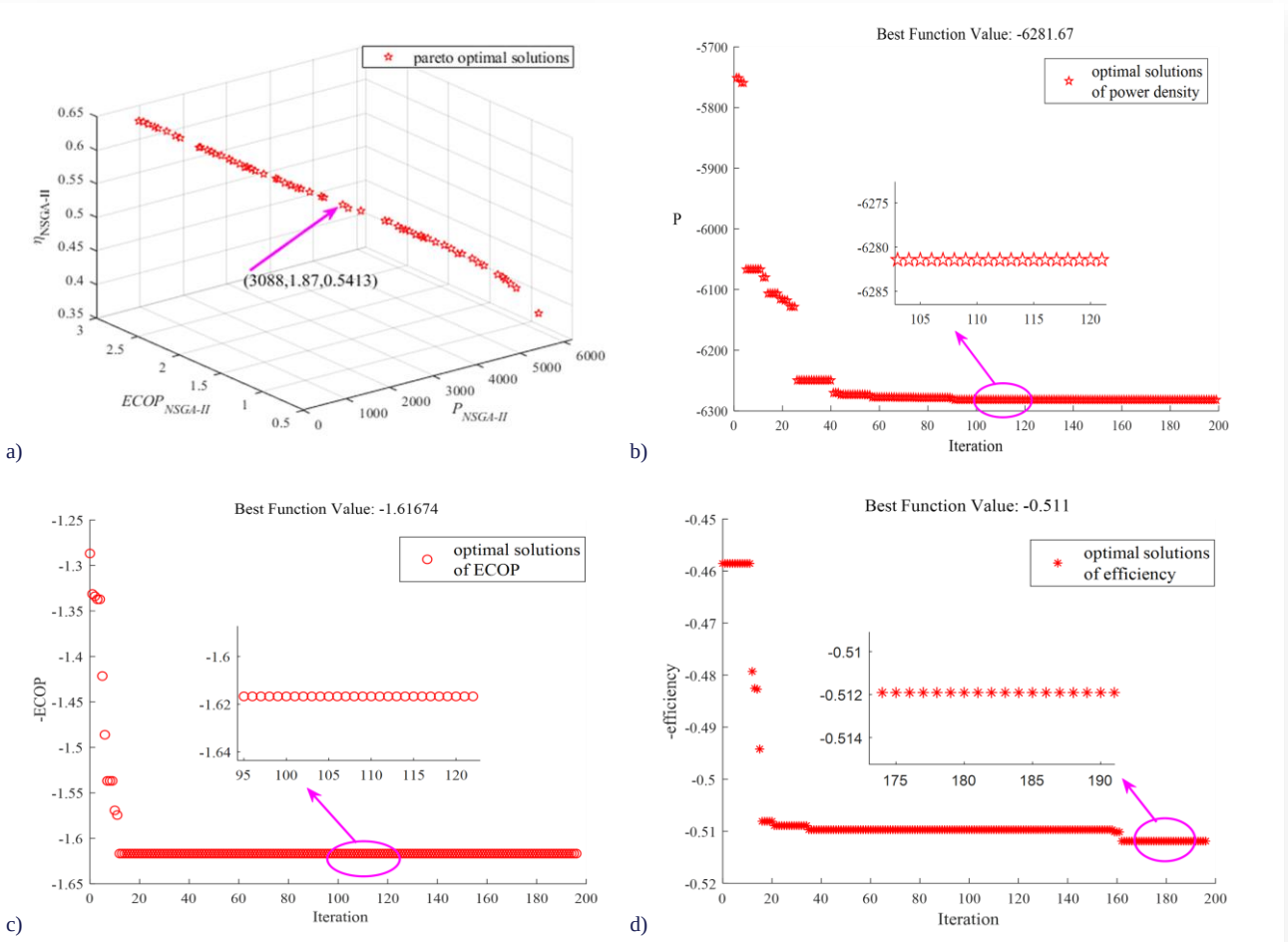

Fig. 8. The optimized Pareto frontier curve of NSGA-II algorithm (a) and the optimization results of the SA algorithm (b-d).

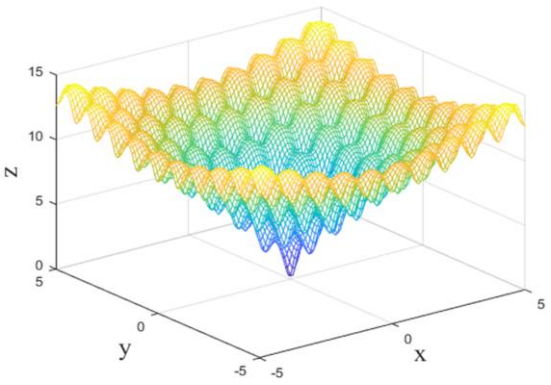

Fig. 9. A graph of the Ackley test function.

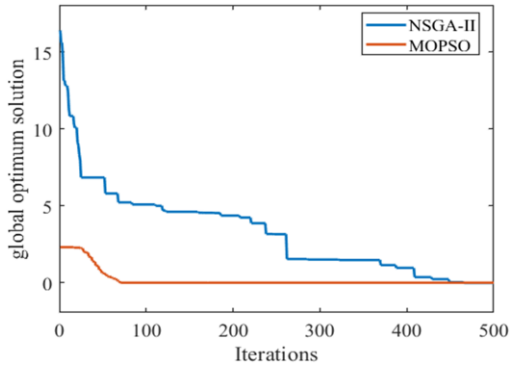

Fig. 10. Comparison of global optimal solutions.

The variation of the global optimal solution with the number of iterations for the MOPSO algorithm and the NSGA-II algorithm for optimization of the Ackley test function is shown in Fig. 10. It can be seen that the MOPSO algorithm finds the global minima within less than 100 iterations, while the NSGA-II algorithm finds the minima only after a number of iterations greater than 400.

Figure 11 shows the variation of the individual (historical) optimal solutions of the MOPSO algorithm and the NSGA-II algorithm with the number of iterations in finding the optimal so-

lution to the Ackley test function when the spatial dimensions of the Ackley test function are taken from the first to the tenth dimension. It can be seen that the MOPSO algorithm is the first to find the extrema in most cases. However, the NSGA-II algorithm always has problems finding local minima, such as in the 1st, 3rd and 10th dimension cases. Moreover, the NSGA-II algorithm shows oscillatory changes in the historical optimal solution when the number of iterations is small.

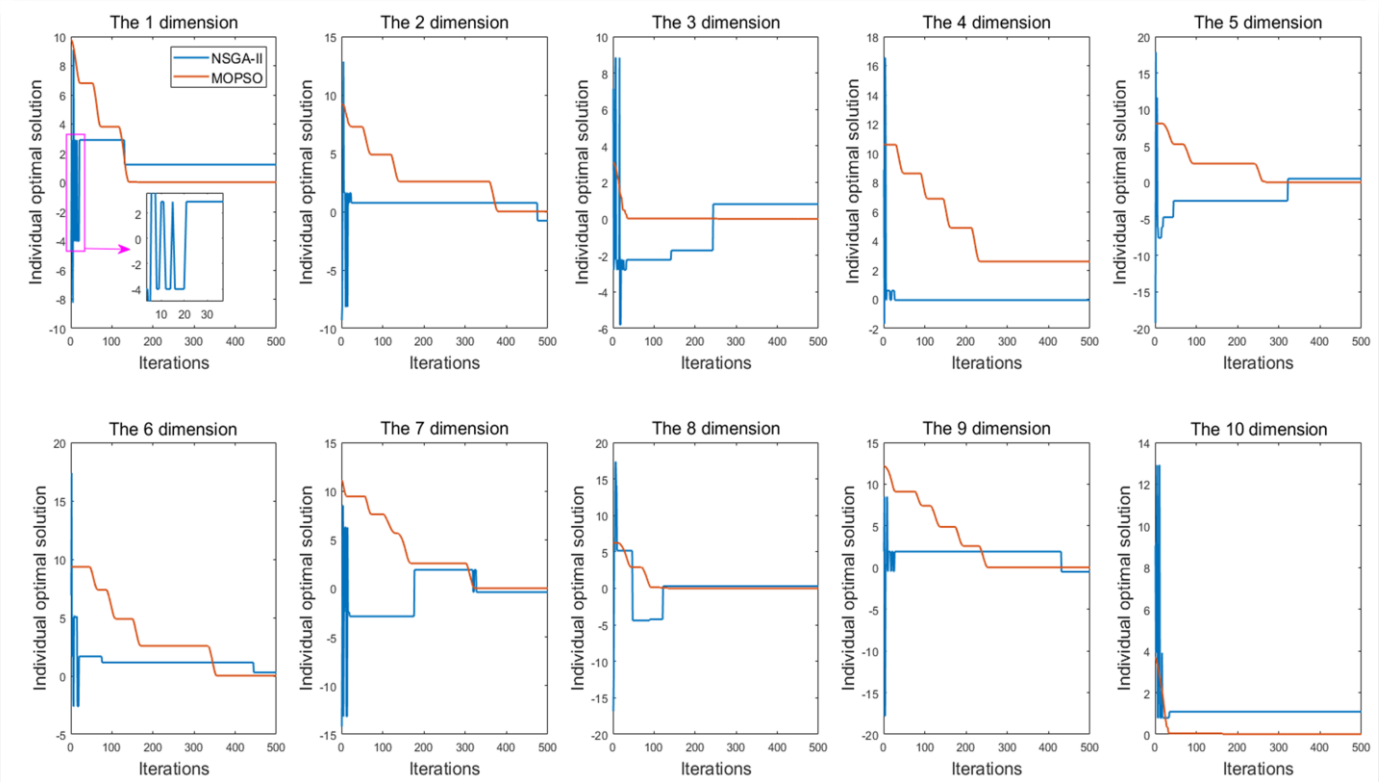

Fig. 11. The variation of the individual (historical) optimal solutions of the MOPSO algorithm and the NSGA-II algorithm.

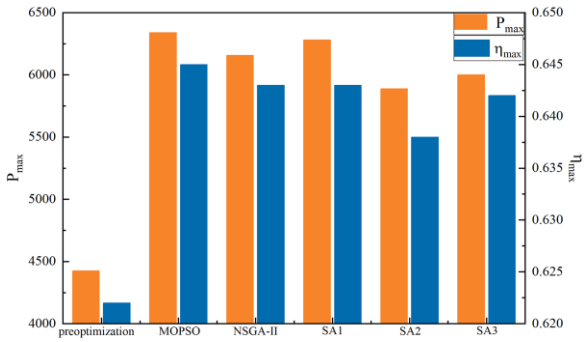

Fig. 12. The optimal result comparison for maximum power density and maximum efficiency.

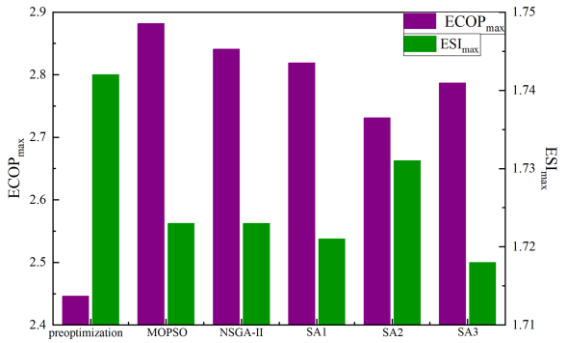

Fig. 13. The optimal result comparison for maximum ECOP and maximum ESI.

From the above results, it can be seen that the MOPSO algorithm is faster in finding the optimum compared to the NSGA-II algorithm and is more accurate and less likely to fall into local extremes.

By using the optimal parameters of the MOPSO algorithm as inputs to the HT-PEMFC model, the obtained maximum power density, maximum efficiency, maximum *ECOP* and maximum *ESI* are compared with the preoptimized results and the results optimized by other algorithms as shown in Figs. 12 and 13. The MOPSO algorithm yields the best performance, with the maximum power density, maximum efficiency, and maximum *ECOP* being 6340 W/m^2, 64.5% and 1.723, respectively, which are 43.28%, 3.7% and 17.8% higher than the preoptimized HT-PEMFC, but the maximum *ESI* is slightly reduced.

4. Conclusions

An irreversible thermodynamic model of HT-PEMFC is established to study the effects of different operating parameters and design parameters on the thermodynamic performance, four parameters including *T*, *DL*, *p*, and *RH* are considered in this work, while *P*, *ECOP* and efficiency are used as the optimization objective functions. The primary findings are summarized as follows:

1) The validation of the irreversible thermodynamic model for HT-PEMFC was conducted through comparison with experimental data.
2) Temperature and pressure have a significant effect on the increase of *P*, *ECOP*, *ESI* and decrease of *EDI*, while *DL* and *RH* have a lesser effect.
3) The population distribution of the optimization variables of the optimal solutions is analyzed based on the 3D Pareto frontier of the MOPSO algorithm, which results in a uniform distribution of the current density in the operating range due to the different weight accounting for each optimization objectives. Temperature and pressure are maintained in the high value region of the operating range, while *DL* is stably distributed between 7 and 8.
4) Parameter optimization of HT-PEMFC using MOPSO algorithm and comparison with the optimization results of NSGA-II algorithm and SA algorithm show that MOPSO algorithm performs well for multi-objective optimization as a function of *P*, *ECOP* and efficiency, with the maximum power density, maximum efficiency, and maximum *ECOP* being 6340 W/m^2, 64.5% and 1.723, respectively, which are 43.28%, 3.7% and 17.8% higher than those of the preoptimized HT-PEMFC.

The conclusions obtained in this paper regarding the future development of HT-PEMFC design and integration into existing systems are: firstly, by considering the effects of temperature and pressure on performance, new membrane electrode materials can be investigated and developed to adapt to operating environments at higher temperatures and pressures, which can help to improve the stability and durability of HT-PEMFC. Secondly, when integrating into an existing system, the effects of operating and design parameters need to be considered, and the system architecture and operating conditions need to be adjusted accordingly, and the MOPSO algorithm can provide guidance for the design of HT-PEMFC systems to achieve optimal performance. In addition, in terms of optimization algorithm selection, future HT-PEMFC developments could consider using the MOPSO algorithm as the preferred parameter optimization algorithm to achieve multi-objective optimization of power, ecological performance and efficiency. By comparing the optimization results of different parameter combinations, the optimal system configuration can be determined to guide future HT-PEMFC development.

Acknowledgements

The research was supported by the financial support of the National Natural Science Foundation of China (No. 51306079 and 51176069), the Postgraduate Research & Practice Innovation Program of Jiangsu Province and Scientific Research Foundation of Nanjing Forestry University (No. GXL2018004).

References

[1] Abdul Rasheed, R.K., Liao, Q., Caizhi, Z., & Chan, S.H. (2017). A review on modelling of high temperature proton exchange membrane fuel cells (HT-PEMFCs). *International Journal of Hydrogen Energy*, 42(5), 3142–3165. doi: 10.1016/j.ijhydene.2016.10.078

[2] Li, Y., Yang, M., Ma, Z., Zheng, M., Song, H., & Guo, X. (2022). Thermodynamic modeling and exergy analysis of a combined High-temperature proton exchange membrane fuel cell and ORC system for automotive applications. *International Journal of Molecular Sciences*, 23(24). doi: 10.3390/ijms232415813

[3] Rosli, R.E., Sulong, A.B., Daud, W R. W., Zulkifley, M.A., Husaini, T., Rosli, M.I., Majlan, E.H., & Haque, M.A. (2017). A review of high-temperature proton exchange membrane fuel cell (HT-PEMFC) system. *International Journal of Hydrogen Energy*, 42(14), 9293–9314. doi: 10.1016/j.ijhydene.2016.06.211

[4] Rosli, R.E., Sulong, A.B., Daud, W.R.W., Zulkifley, M.A., Husaini, T., Rosli, M.I., Majlan, E.H., & Haque, M.A. (2017). Modeling and analysis of a 5 kW HT-PEMFC system for residential heat and power generation. *International Journal of Hydrogen Energy*, 42(3), 1698–1714. doi: 10.1016/j.ijhydene.2016.10.152

[5] Yang, M., & Tian, J. (2023). Longitudinal and Lateral Stability Control Strategies for ACC Systems of Differential Steering Electric Vehicles. *Electronics*, 12(19). doi: 10.3390/electronics12194178

[6] Chen, Z., Zuo, W., Zhou, K., Li, Q., Huang, Y., & E, J. (2023). Multi-factor impact mechanism on the performance of high temperature proton exchange membrane fuel cell. *Energy*, 278, 127−982. doi: 10.1016/j.energy.2023.127982

[7] Lei, G., Zheng, H., Zhang, J., Siong Chin, C., Xu, X., Zhou, W., & Zhang, C. (2023). Analyzing characteristic and modeling of high-temperature proton exchange membrane fuel cells with CO poisoning effect. *Energy*, 282, 128−305. doi: 10.1016/j.energy.2023.128305

[8] Jannat, S., Rashtchi, H., Atapour, M., Golozar, M.A., Elmkhah, H., & Zhiani, M. (2019). Preparation and performance of nanometric Ti/TiN multi-layer physical vapor deposited coating on 316L stainless steel as bipolar plate for proton exchange membrane fuel cells. *Journal of Power Sources*, 435, 226−818. doi: 10.1016/j.jpowsour.2019.226818

[9] Salimi Nanadegani, F., Nemati Lay, E., & Sunden, B. (2020). Computational analysis of the impact of a micro porous layer (MPL) on the characteristics of a high temperature PEMFC. *Electrochimica Acta*, 333, 135−552. doi: 10.1016/j.electacta.2019.135552

[10] Atak, N.N., Dogan, B., & Yesilyurt, M.K. (2023). Investigation of the performance parameters for a PEMFC by thermodynamic analyses: Effects of operating temperature and pressure. *Energy*, 282, 128907. doi: 10.1016/j.energy.2023.128907

[11] Chen, X., Xu, J., Yang, C., Fang, Y., Li, W., Zhang, Y., Wan, Z., & Wang, X. (2021). Thermodynamic and economic study of PEMFC stack considering degradation characteristic. *Energy Conversion and Management*, 235. doi: 10.1016/j.enconman.2021.114016

[12] Lu, X., Du, B., Zhu, W., Yang, Y., Xie, C., Tu, Z., Zhao, B., Zhang, L., Song, J., & Deng, Z. (2023). Thermodynamic and dynamic analysis of a hybrid PEMFC-ORC combined heat and power (CHP) system. *Energy Conversion and Management*, 292, 117408. doi: 10.1016/j.enconman.2023.117408

[13] Özgür, T., & Yakaryilmaz, A. C. (2018). Thermodynamic analysis of a Proton Exchange Membrane fuel cell. *International Journal of Hydrogen Energy*, 43(38), 18007−18013. doi: 10.1016/j.ijhydene.2018.06.152

[14] Wang, B., Wu, K., Xi, F., Xuan, J., Xie, X., Wang, X., & Jiao, K. (2019). Numerical analysis of operating conditions effects on PEMFC with anode recirculation. *Energy*, 173, 844−856. doi: 10.1016/j.energy.2019.02.115

[15] Xia, S., Lin, R., Cui, X., & Shan, J. (2016). The application of orthogonal test method in the parameters optimization of PEMFC

under steady working condition. *International Journal of Hydrogen Energy*, 41(26), 11380−11390. doi: 10.1016/j.ijhydene.2016.04.140

[16] Chen, X., Li, W., Gong, G., Wan, Z., & Tu, Z. (2017). Parametric analysis and optimization of PEMFC system for maximum power and efficiency using MOEA/D. *Applied Thermal Engineering*, 121, 400−409. doi: 10.1016/j.applthermaleng.2017.03.144

[17] Xu, H., Song, H., Xu, C., Wu, X., & Yousefi, N. (2020). Exergy analysis and optimization of a HT-PEMFC using developed Manta Ray Foraging Optimization Algorithm. *International Journal of Hydrogen Energy*, 45(55), 30932−30941. doi: 10.1016/j.ijhydene.2020.08.053

[18] Lin, D., Yehong, H., & Khodaei, H. (2020). Application of the meta-heuristics for optimizing exergy of a HT-PEMFC. *International Journal of Energy Research*, 44(5), 3749−3761. doi: 10.1002/er.5163

[19] Ehyaei, M.A., Ahmadi, A., El Haj Assad, M., & Salameh, T. (2019). Optimization of parabolic through collector (PTC) with multi objective swarm optimization (MOPSO) and energy, exergy and economic analyses. *Journal of Cleaner Production*, 234, 285−296. doi: 10.1016/j.jclepro.2019.06.210

[20] Yuan, X., Liu, Y., & Bucknall, R. (2021). Optimised MOPSO with the grey relationship analysis for the multi-criteria objective energy dispatch of a novel SOFC-solar hybrid CCHP residential system in the UK. *Energy Conversion and Management*, 243. doi: 10.1016/j.enconman.2021.114406

[21] Thosar, A.U., Agarwal, H., Govarthan, S., & Lele, A.K. (2019). Comprehensive analytical model for polarization curve of a PEM fuel cell and experimental validation. *Chemical Engineering Science*, 206, 96−117. doi: 10.1016/j.ces.2019.05.022

[22] Guo, Y., Guo, X., Zhang, H., & Hou, S. (2020). Energetic, exergetic and ecological analyses of a high-temperature proton exchange membrane fuel cell based on a phosphoric-acid-doped polybenzimidazole membrane. *Sustainable Energy Technologies and Assessments*, doi: 10.1016/j.seta.2020.100671

[23] Li, D., Li, S., Ma, Z., Xu, B., Lu, Z., Li, Y., & Zheng, M. (2021). Ecological Performance Optimization of a High Temperature Proton Exchange Membrane Fuel Cell. *Mathematics*, 9(12). doi: 10.3390/math9121332

[24] Scott, K., Pilditch, S., & Mamlouk, M. (2007). Modelling and experimental validation of a high temperature polymer electrolyte fuel cell. *Journal of Applied Electrochemistry*, 37(11), 1245−1259. doi: 10.1007/s10800-007-9414-1